Please find the published version at:
https://www.sciencedirect.com/science/article/pii/S030626192031309X#

Steam ejector performance considering phase transition for multi-effect distillation with thermal vapour compression (MED-TVC) desalination system

Chuang Wen[1], Liang Gong[2], Hongbing Ding[3], Yan Yang[1, *]

[1]Faculty of Engineering, University of Nottingham, Nottingham NG7 2RD, United Kingdom

[2]College of New Energy, China University of Petroleum (East China), Qingdao, Shandong 266580, China

[3]Tianjin Key Laboratory of Process Measurement and Control, School of Electrical and Information Engineering, Tianjin University, Tianjin 300072, China

*Corresponding author: Yan Yang, Email: yan.yang1@nottingham.ac.uk; flyloveyang@gmail.com

Abstract: The multi-effect distillation with thermal vapour compression (MED-TVC) desalination system is efficient to produce freshwater. The steam ejector performance is not fully understood as the phase transition has been ignored in many studies. The present work develops a two-phase condensing flow model to assess the steam ejector performance considering nonequilibrium condensation phenomena. The transition of the flow structure from an under-expanded flow to an over-expanded flow in the steam ejector is investigated in detail. We present that the maximum Mach number can reach 4.02 in the under-expanded flow, which is weakened to 2.88 in the over-expanded flow. The steam undergoes several expansion-compression processes in the steam ejector in the under-expanded flow, which induces the formation and evaporation of massive

droplets. In the over-expanded flow, the steam is compressed and then expanded after leaving the primary nozzle and the condensation process is not observed in mixing and constant sections. The increasing suction chamber pressure significantly improves the entrainment ratio while leading to an increasing entropy loss coefficient. The entrainment ratio is improved from 0.25 for the under-expanded flow to 1.69 for the over-expanded flow, while the entropy loss increases from 0.081 for the under-expanded flow to 0.29 for the over-expanded flow. This indicates that the transition of the flow structure from an under-expanded flow to an over-expanded flow can entrain more steam from the last effect while causes more entropy losses in a steam ejector for the MED-TVC desalination system.

Keywords: multi-effect distillation (MED); thermal vapour compression (TVC); steam ejector; nonequilibrium condensation; entropy loss; entrainment ratio

1. Introduction

The desalination technologies [1, 2] contribute to the production of freshwater to combat the crisis of water resources. The multi-effect distillation with thermal vapour compression (MED-TVC) desalination system has been used to produce freshwater with the advantages of energy recoveries [3] and high technological economy [4, 5]. Elsayed et al. [6] carried out an economical investigation on the MED-TVC desalination system based on four different feed configurations. The simulation results showed that the parallel crossfeed method could obtain a preferable economical efficiency than backward, forward and parallel feed methods. Askari & Mehran [7] integrated solar fields to the MED-TVC desalination system as thermal sources and

their economical analysis showed that the freshwater production cost was increased due to the integration of solar energy. Khalid et al. [8] studied the role of TVC locations in the MED-TVC unit based on forward and parallel feed methods. They found that the best performance could be obtained by locating the TVC unit in the middle desalination system.

The TVC unit, also known as a steam ejector [9, 10] in the desalination system, can recover the low-pressure steam [11-13]. The TVC performance has been evaluated and demonstrated in various experimental studies. Sharifi & Boroomand [14] experimentally measured the entrainment ratios under real operational conditions in a MED-TVC desalination field, which has been used for the validation of the numerical study [15]. The two-stage vacuum ejectors were designed to improve the MED-TVC system performances [16]. Han et al. [17] improved the ejector performance with preheated secondary flows, and their experiments demonstrated that the entrainment ratio could be increased by 31% with superheated secondary steam of 15 °C.

The computational fluid dynamics (CFD) modellings were utilised for the design, optimisation and evaluation on the steam ejector. Tang et al. [18] used the pressure regulation to optimise a steam ejector, which could improve the entrainment ratio by 11.77%. In another study, the numerical simulation improved the entrainment ratio by 28.75% via combining the pressure regulation and entrainment passages to the steam ejector [19]. A new steam ejector for the MED-TVC unit was proposed with an adaptive nozzle exit position, which increased 36% entrainment ratio by adjusting the nozzle exit position [20]. Park [21] introduced the swirling flow nozzles to optimise a steam

ejector in MED-TVC units. The variable geometry ejectors were designed to improve an averaged entrainment ratio by more than 100% [22]. Liu et al. [23] numerically studied the influences of the area ratio on an ejector and the entrainment ratio could be improved dramatically by changing the area ratio. Wang et al. [24] computationally optimised a primary nozzle in a steam ejector and it was found that an ejector overall efficiency was improved by approximately 14%. The abovementioned numerical studies employed the dry gas model and ignored the phase change process in a steam ejector.

Sharifi et al. [25] numerically compared the dry gas and wet steam models for a steam ejector and they found that the condensing flow reduced the peak Mach number and improved ejector performances. Mazzelli et al. [26] performed a detailed validation and sensitivity analysis on the condensing flow model and showed that the liquid fraction could reach 0.2 in a steam ejector. The visualization experiment was carried out to observe the nonequilibrium condensation in a steam ejector [27]. Their experiments demonstrated that the condensed droplets were nonuniform in supersonic flows. Our previous study [28] demonstrated that a dry gas model caused an unphysical temperature distribution inside an ejector and under-predicted the entropy loss by 15% than the nonequilibrium condensing flow model. These studies indicate that the phase transition processes are important for the ejector performances for the MED-TVC desalination system.

Considering the aforementioned literature surveys, the novelty of this work is:

1) A two-phase condensing flow model is developed to study ejector performances

for the MED-TVC systems considering phase transition processes with the condensation and evaporation of massive droplets in supersonic flows.

2) The nonequilibrium condensation processes in the under-expanded and over-expanded supersonic flows are carried out in a steam ejector for the MED-TVC desalination system.

3) The entrainment performance and entropy loss are investigated during the transition of the flow structure from under-expanded to over-expanded flows in the steam ejector for the MED-TVC desalination system using the condensing flow model.

The results from the study provide a quantitative assessment of the transition of the flow structure from an under-expanded flow to an over-expanded flow with heat and mass transfer during the phase transition in supersonic flows. This can be used for the design and operation of a steam ejector, which upgrades the low-grade energy for the MED-TVC desalination system.

2. Problem statement

2.1. The MED-TVC desalination system and steam ejector

Figure 1 describes a MED-TVC desalination system, in which a steam ejector is used to recirculate part of the steam from the last effect [23]. The expansion level of the high-pressure steam inside the primary nozzle depends on the area ratio between the nozzle exit ad nozzle throat. The pressure difference between the nozzle outlet and the suction chamber determines the flow structures downstream the primary nozzle. In this study, the diameters of the throat and exit of the primary nozzle are 2.00 mm and 8.00, respectively. The inlet diameter of the mixing and constant sections are 24.00 mm and

19.00 mm, respectively. The other dimensions can be found in Table 1 [29, 30], which is specifically designed to efficiently entrain the low-pressure steam from the last effect.

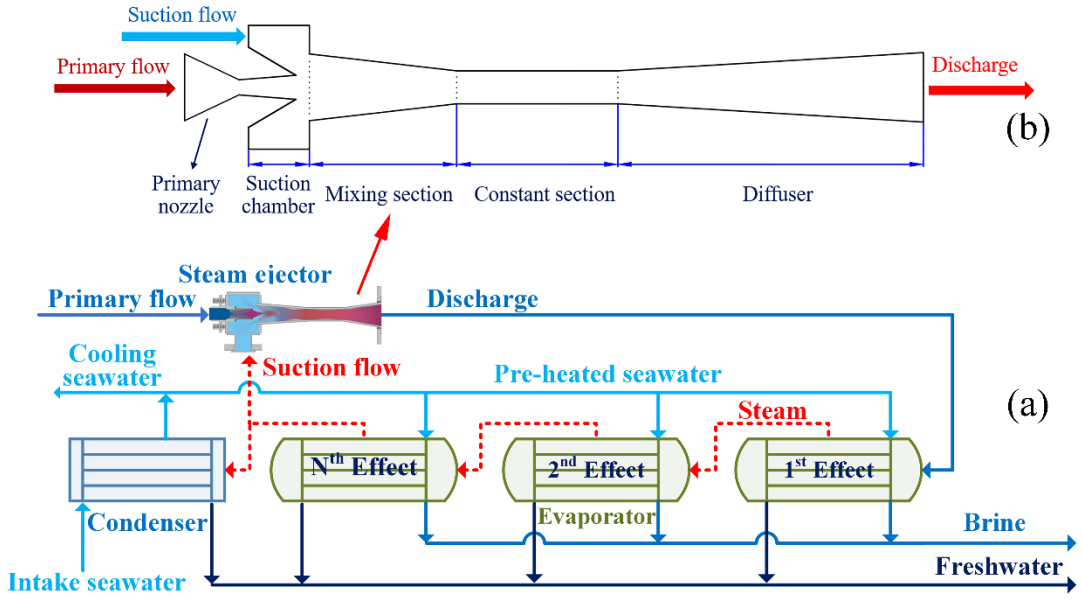

Fig. 1 Steam ejector and MED-TVC desalination system

Table 1 Detailed dimension for the steam ejector [29, 30]

Steam ejector dimension	Size (mm)
Primary nozzle: inlet diameter	7.76
Primary nozzle: throat diameter	2.00
Primary nozzle: outlet diameter	8.00
Primary nozzle: length of the converging portion	12.00
Primary nozzle: length of the diverging portion	34.29
Mixing section: inlet diameter	48.00
Mixing section: length	130.00
Constant section: diameter	19.00
Constant section: length	95.00
Diffuser: outlet diameter	40.00
Diffuser: length of the diffuser	180.00

2.2. Mathematical modelling

The unsteady, compressible Navier-Stokes equations are employed to govern the fluid flow in a steam ejector considering the nonequilibrium condensation process [31, 32]. The numerical modelling is developed with following assumptions: (1) a single-

fluid model is used with neglecting slip velocities between vapour and liquid phases [33, 34]; (2) there are no temperature differences between vapour and liquid phases [35]; (3) condensed droplets distribute uniformly in the vapour phase [36]. The governing equations are expressed as:

$$\frac{\partial(H)}{\partial t}+\frac{\partial\left(U_x\right)}{\partial x}+\frac{\partial\left(U_y\right)}{\partial y}=\frac{\partial\left(J_x\right)}{\partial x}+\frac{\partial\left(J_y\right)}{\partial y}+S \tag{1}$$

where

$$H=\begin{bmatrix}\rho\\ \rho u\\ \rho v\\ \rho E\\ \rho\zeta\\ \rho N\end{bmatrix},U_x=\begin{bmatrix}\rho u\\ \rho uu+p\\ \rho uv\\ \rho u(E+p)\\ \rho u\zeta\\ \rho uN\end{bmatrix},U_y=\begin{bmatrix}\rho v\\ \rho uv\\ \rho vv+p\\ \rho v(E+p)\\ \rho v\zeta\\ \rho vN\end{bmatrix} \tag{2}$$

$$J_x=\begin{bmatrix}0\\ \tau_{xx}\\ \tau_{xy}\\ q_x\\ 0\\ 0\end{bmatrix},J_y=\begin{bmatrix}0\\ \tau_{xy}\\ \tau_{yy}\\ q_y\\ 0\\ 0\end{bmatrix},S=\begin{bmatrix}-\dot{m}\\ -u\dot{m}\\ -v\dot{m}\\ -(h_v-h_{fg})\dot{m}\\ \dot{m}\\ \rho I\end{bmatrix} \tag{3}$$

where H represents conservation variables, U and J are inviscid and viscid fluxes, S is the source term. ζ and N are the liquid fraction and droplet numbers. ρ and p are density and pressure. E is the total energy, u and v are the velocity components. I is the nucleation rate [37]. $\dot{m}$ is the condensation mass rate [38, 39]:

$$\dot{m}=\frac{4\pi r_c^{\,3}}{3}\rho_l I+4\pi r^2\rho_l N\frac{dr}{dt} \tag{4}$$

$$I=\frac{q_c}{1+\phi}\frac{\rho_v^{\,2}}{\rho_l}\sqrt{\frac{2\sigma}{\pi m_v^{\,3}}}\exp\left(-\frac{4\pi\sigma}{3k_BT_v}r_c^{\,2}\right) \tag{5}$$

$$\frac{dr}{dt}=\frac{\lambda_v\left(T_s-T_v\right)}{\rho_l h_{lv}r}\frac{\left(1-r_c/r\right)}{\left(\frac{1}{1+2\beta\mathrm{Kn}}+3.78(1-\nu)\frac{\mathrm{Kn}}{\mathrm{Pr}}\right)} \tag{6}$$

The UDF and UDS are employed to interpret the liquid fraction (ζ) and droplet number (N) equations and source terms to ANSYS FLUENT 19 [40]. Considering the complicated flow structure in the steam ejector, the shear stress transport (SST) k-ω turbulence model is used for the performance evaluation of a steam ejector for the MED-TVC desalination system [41]. The total pressure and total temperature boundary conditions are employed for the entrances and exit of the steam ejector. Figure 2 shows the quadrilateral grids for the steam ejector and the mesh independent tests are shown in Fig. 3 using 39000, 73000 and 168000 cells, respectively. The pressure distribution computed by the coarse mesh is different from the ones calculated by the other two meshes. The coarse grid also computes a maximum nucleation rate of 1.07×10^{25} m^{-3} s^{-1} compared to 4.47×10^{26} m^{-3} s^{-1} and 4.78×10^{26} m^{-3} s^{-1} for medium and fine grids. This indicates that the medium and fine grids show a better performance in the prediction of the flow structure compared to the coarse mesh. Furthermore, the medium mesh predicts similar flow behaviour and entrainment ratio compared to the fine mesh. Considering numerical accuracies and costs, the medium mesh is suggested for ejector evaluations in the MED-TVC desalination system.

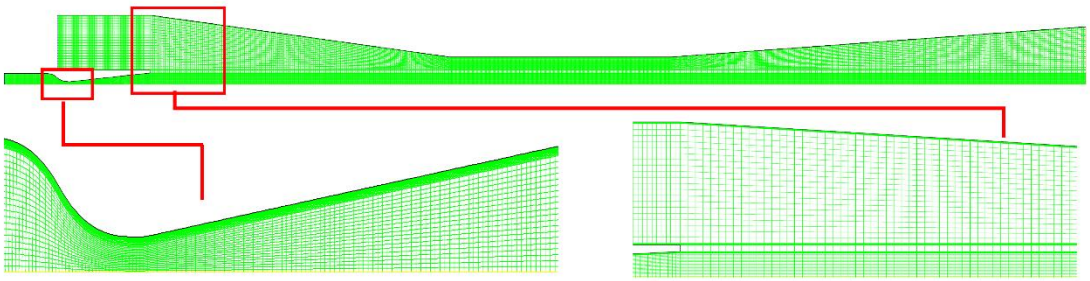

Fig. 2 Quadrilateral grid of the steam ejector

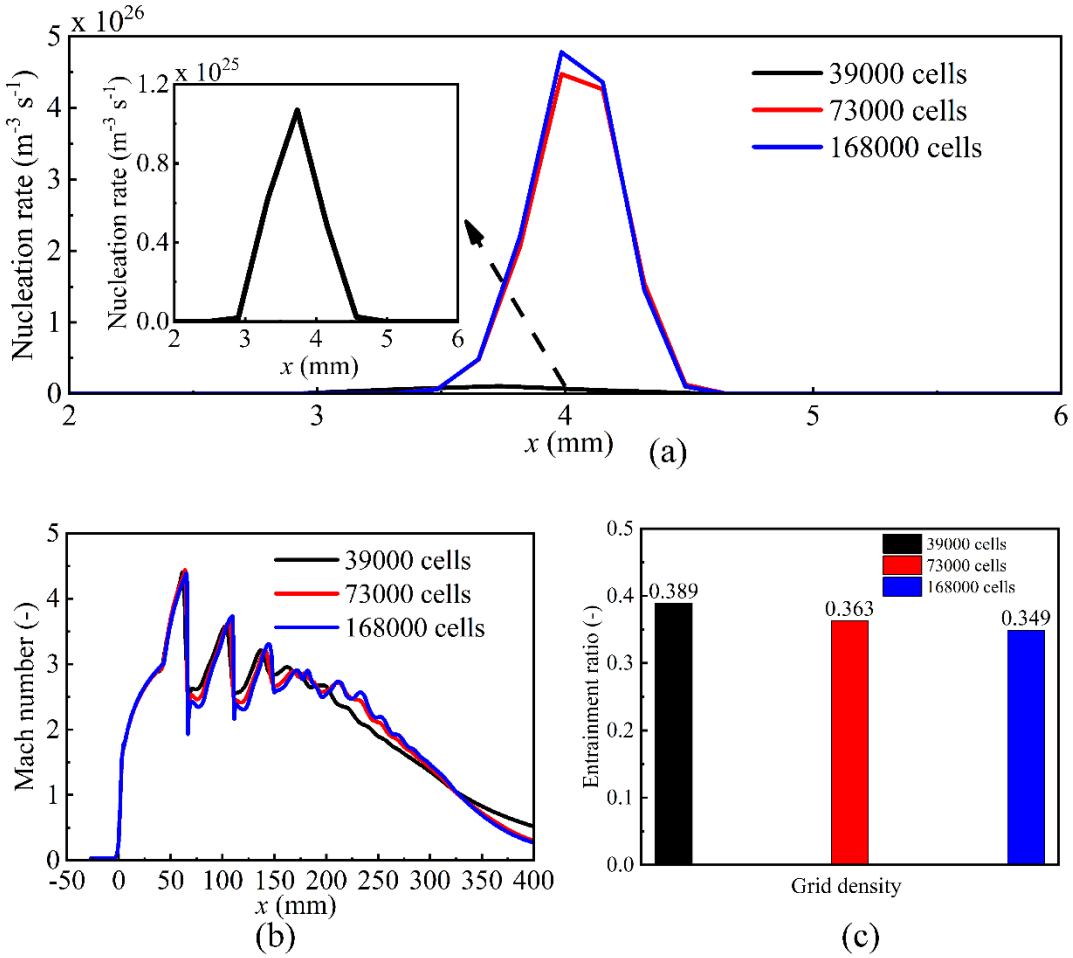

Fig. 3 Mesh independence results of the steam ejector

3. Results and discussion

3.1. Model validation

The Laval nozzle (Case 203) [42, 43] is utilised to validate the nonequilibrium condensing model. The root-mean-square (R^2), which is defined in Eq. (7), is used to compare the numerical and experimental errors [44-46]. Figure 4 shows the computed and experimental pressure and droplet radius, as well as the relative errors. The computational pressure agrees with experimental data and the Wilson point is accurately obtained by the developed CFD modelling. The calculated droplet radius is smaller than experimental data with a relative error of less than 15%. Thus, the

developed wet steam model accurately evaluates nonequilibrium condensations inside supersonic flows.

$$R^2 = 1 - \frac{\sum_{i=1}^{n}(a_i - p_i)^2}{\sum_{i=1}^{n}(p_i)^2} \tag{7}$$

where a_i and p_i are experimental and numerical values.

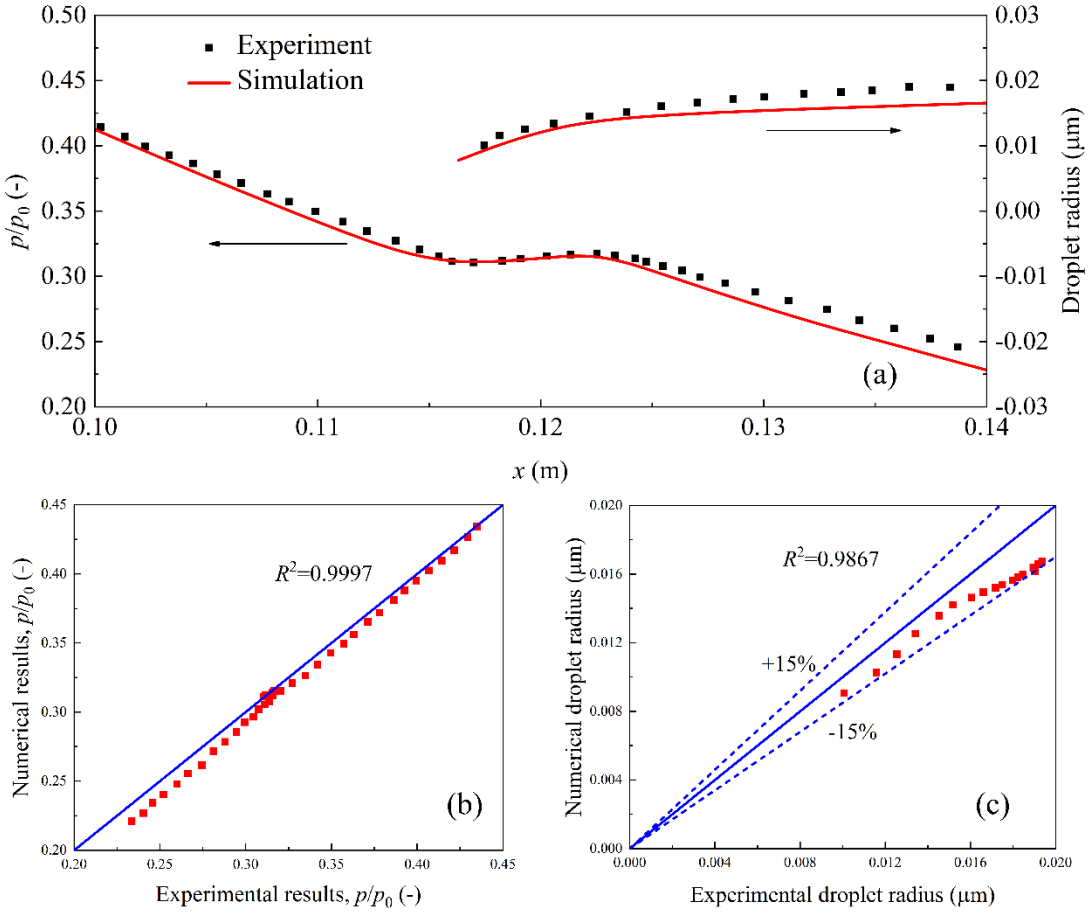

Fig. 4 Wet steam modelling validation in Laval nozzles: (a) numerical and experimental pressure and droplet radius, (b) error analysis of pressure, and (c) error analysis of droplet radius

The CFD modelling is further validated for the steam ejector against the experiments carried out by Sriveerakul et al. [29, 30]. The numerical and experimental results and the relative error are described in Fig. 5. The computed entrainment ratio of 0.294 is

lower than the experimental measurement of 0.31 with a relative error of 5.12%. Furthermore, the predicted pressures are higher than the experimental one when the measured values are less than 860 Pa. This has been attributed to the difficulty of calibrating the absolute pressure transducer near absolute zero levels [29, 30]. And the predicted pressures in the diffuser where they are greater than 1000 Pa are in good with the measurements in the steam ejector. Therefore, the developed nonequilibrium condensing flow model can be used for the performance evaluation of a steam ejector.

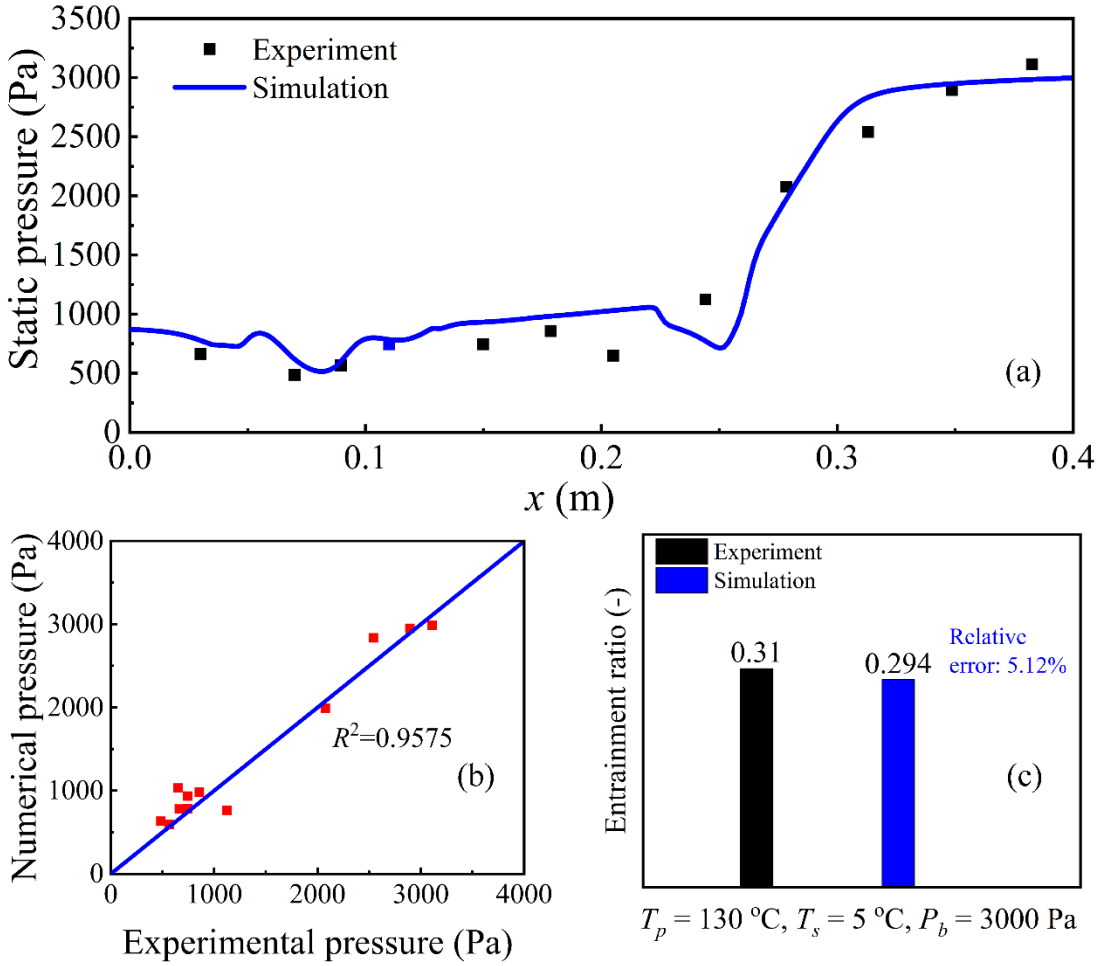

Fig. 5 CFD validation for steam ejectors: (a) computed and experimental results, (b) error analysis of pressure and (c) entrainment ratios for the simulation and experiment

3.2. Under-expanded and over-expanded flows in steam ejectors

The high-pressure steam accelerates inside the primary nozzle converging part, chokes at the throat and reaches a supersonic velocity in the diverging part. The steam will then enter the mixing section, which characterises an under-expansion flow or over-expanded flow depending on mixing section pressures. Fig. 6 represents a flow structure inside the steam ejector at the suction chamber pressure from 850 pa to 5000 Pa. Fig. 6 (a) shows that the nozzle exit pressures are much higher than the surrounding pressure in the mixing section, which results in an under-expansion flow with a large divergence angle of the expansion wave. This results in a higher supersonic flow, which can be demonstrated by the increasing Mach number to approximately 4.02 at the suction chamber pressure of 850 Pa. This subsequently generates higher expansion-compression processes in the mixing section accompanied by oblique waves.

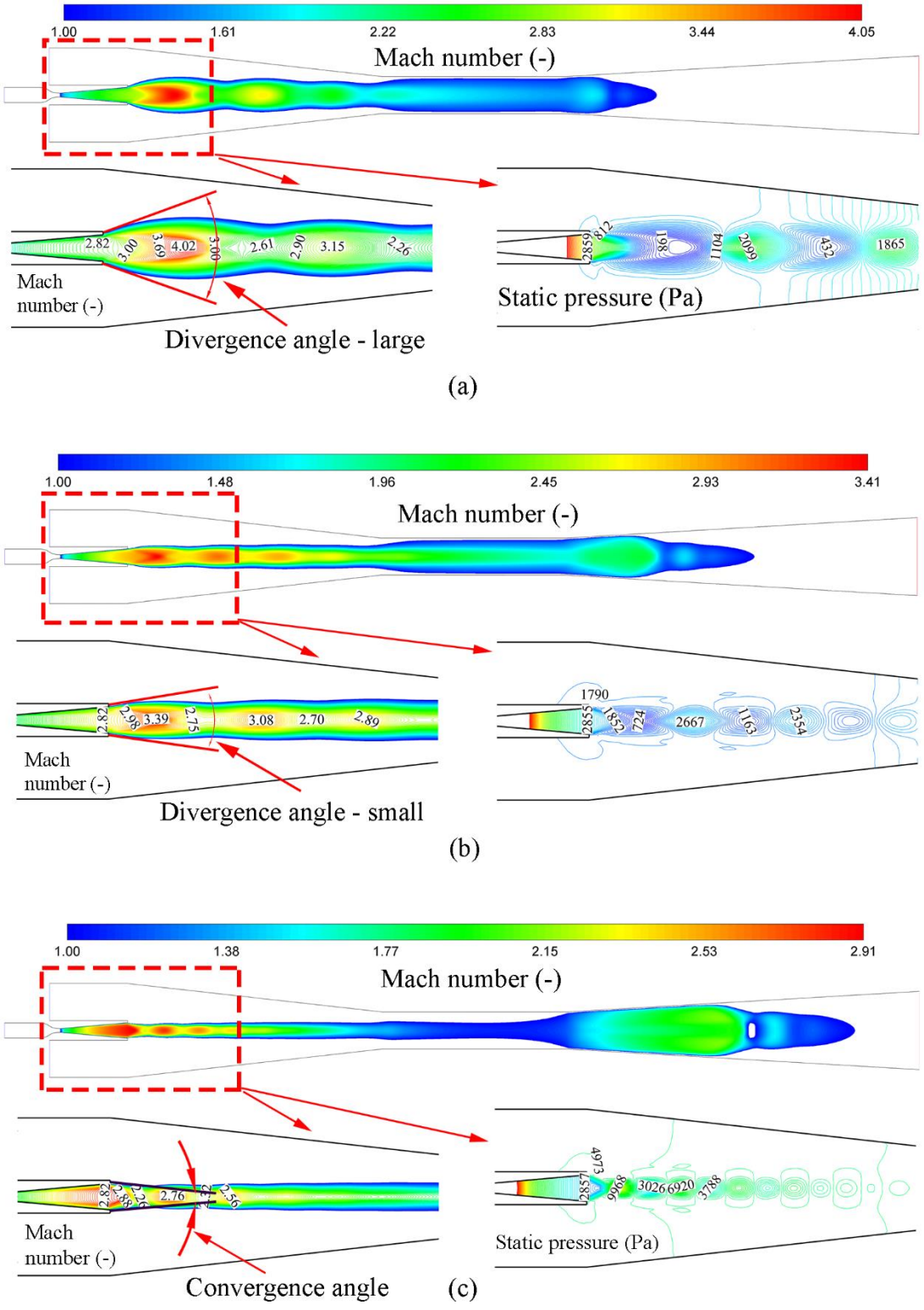

Fig. 6 Flow structure in the steam ejector: (a) high under-expanded flows, (b) slight under-expanded flows, and (c) over-expanded flows

The expansion level of the steam downstream the primary nozzle is diminished

because of the increase of the surrounding pressure in the mixing section when the suction chamber pressure is 1800 Pa in Fig. 6 (b). The divergence angle of the expansion flow becomes smaller compared to the high expansion flows in Fig. 6 (a). This subsequently decreases the maximum Mach number, which is decreased to approximately 3.39 in this case. When the suction chamber pressure increases to 5000 Pa, the surrounding pressure in the mixing section is about 4973, which is higher than the nozzle outlet pressure of 2857 Pa. This results in a significant change of the flow structure downstream the primary nozzle inside the mixing section of the ejector in Fig. 6 (c), which is quite different from the other two cases in Fig. 6 (a) and Fig. 6 (b). It can be observed that the flow structure characterises an over-expanded flow in the mixing section with a convergence angle, which further diminishes the supersonic level of the steam flow with a maximum Mach number of around 2.88. This indicates that the steam represents different expansion levels due to the surrounding pressure in the mixing section, which illustrates the transition of the flow structure from under-expanded to over-expanded flows inside the steam ejector with an increasing suction chamber pressure.

3.3. Nonequilibrium condensations in under-expanded and over-expanded flows

In this section, the nonequilibrium condensation phenomenon is analysed in under-expanded and over-expanded flows in the steam ejector. Figures 7 – 10 describe the condensing flow parameters in the steam ejector at various suction chamber inlet pressures. The steam shows same nonequilibrium condensation behaviour in the primary nozzle under different inlet pressures of the suction chamber of 850 pa, 1800

pa and 5000 Pa. The steam achieves a maximum degree of subcooling of approximately 40 K inside primary nozzle divergent parts to generate first condensations with a maximum nucleation rate of about 9.87×10^{24} m^{-3} s^{-1}. The dramatic nonequilibrium state of the steam leads to a high droplet growth rate. The liquid fraction reaches around 0.14 at the primary nozzle exit for these three cases. This indicates that the nonequilibrium condensations inside the primary nozzles are not influenced by suction chamber inlet pressures due to the huge pressure difference between the motive flows and the secondary flows.

For two under-expanded flow cases of the suction chamber pressures of 850 Pa and 1800 Pa, the nonequilibrium condensation process represents similar characteristics in the mixing and constant sections, while some slight differences are observed. The steam presents several expansion-compression processes in the mixing and constant sections for both two cases. When the suction chamber pressure is 850 Pa, the under-expanded flow achieves four expansion-compression processes, which induces four processes of the transition from the supersaturation state to the subsaturation state of the steam. The maximum liquid fraction can reach 0.20 for the inlet pressure of 850 Pa. Due to the energy loss of the expansion-compression process, the expansion level of the steam is weakened compared to the previous one. For instance, the maximum degrees of subcooling are about 50 K, 25 K, 16 K and 10 K, respectively. However, only the first two expansion processes induce the nonequilibrium condensations during four expansion-compression processes. Similarly, five expansion-compression processes are observed for the suction chamber inlet pressure of 1800 Pa. The maximum

degrees of subcooling are 30 K, 17 K, 11 K, 7 K and 8 K, respectively. Under these conditions, only one nucleation process is observed in the first expansion-compression process in the mixing and constant sections.

In the over-expanded flow, on the contrary, the steam represents five compression-expansion processes inside the mixing and constant sections, which induces a peak degree of subcooling of approximately 19 K. The condensation processes are not observed in the mixing section for this case. Combined with the Mach numbers in Fig. 6, the shock wave shifts further downstream in the diffuser during the transition of the flow structure from under-expanded flows to over-expanded flows. Subsequently, the over-expanded flow allows the steam to further expand in the diffuser, which triggers another extremely nonequilibrium state of the steam in the diffuser and the peak degree of subcooling reaches approximately 60 K. This induces another nucleation process in the diffuser in the over-expanded flow case, which is not observed in other two under-expanded flow cases.

For both under-expanded and over-expanded flows in the mixing and constant sections, the growth rate of the droplet varies alternatively with a positive value for the expansion process and a negative value for the compression process, which characterises the formation and evaporation of the condensed droplets. This is also demonstrated by the distributions of the liquid fraction, which increases in the expansion process and decreases in the compression process in the steam ejector. Furthermore, by combining these three cases of under-expansion and over-expanded flows, it illustrates that the nucleation process only can be launched when the degree of

subcooling is greater than 19 K. This demonstrates that the nucleation and condensation processes will occur in an extremely nonequilibrium state of the steam in the steam ejector.

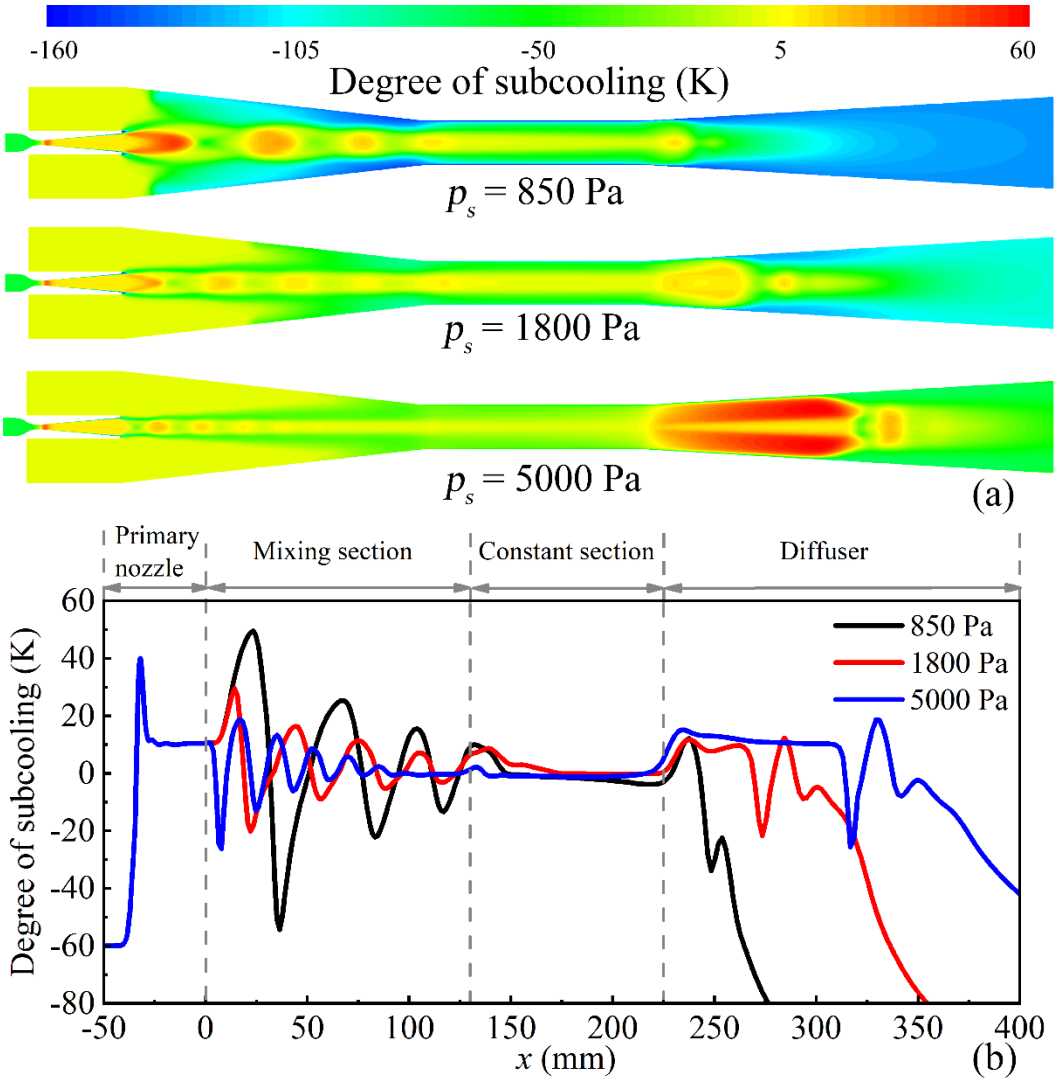

Fig. 7 Impacts of the suction chamber pressure on nonequilibrium condensations in under-expanded and over-expanded flows inside the steam ejector: (a) contours and (b) profiles of the degree of subcooling

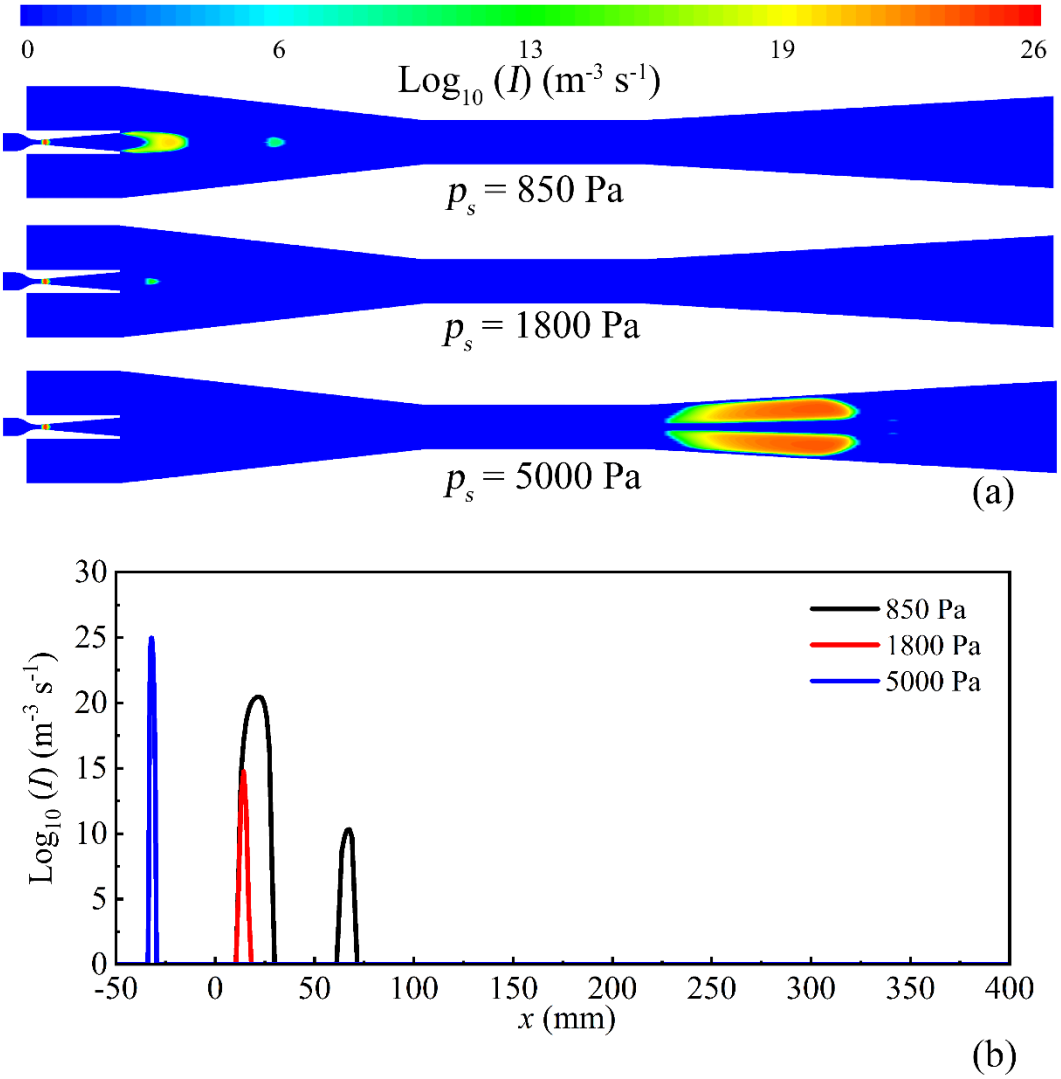

Fig. 8 Impacts of the suction chamber pressure on nonequilibrium condensations in under-expanded and over-expanded flows inside the steam ejector: (a) contours and (b) profiles of nucleation rate

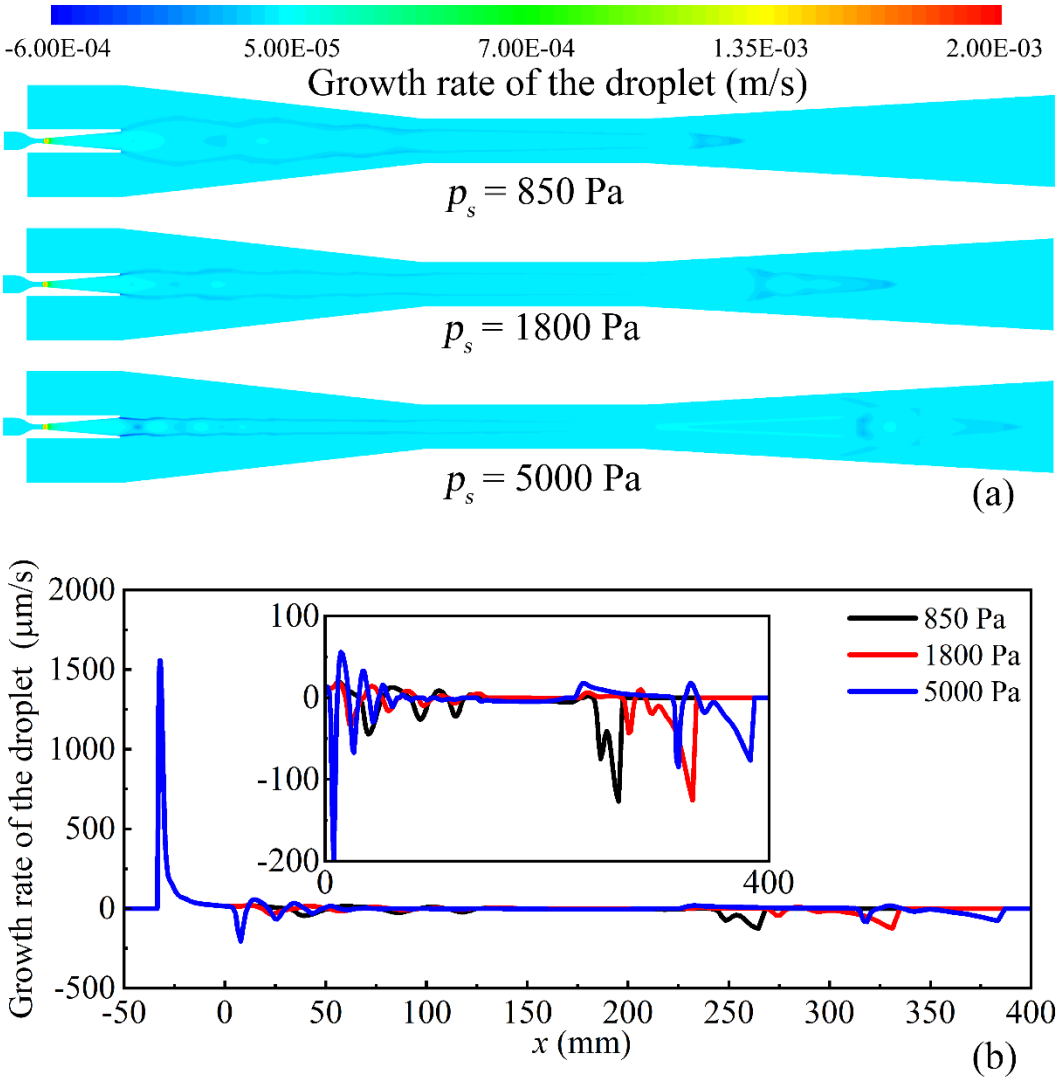

Fig. 9 Impacts of the suction chamber pressure on nonequilibrium condensations in under-expanded and over-expanded flows inside the steam ejector: (a) contours and (b) profiles of the growth rate of the droplet

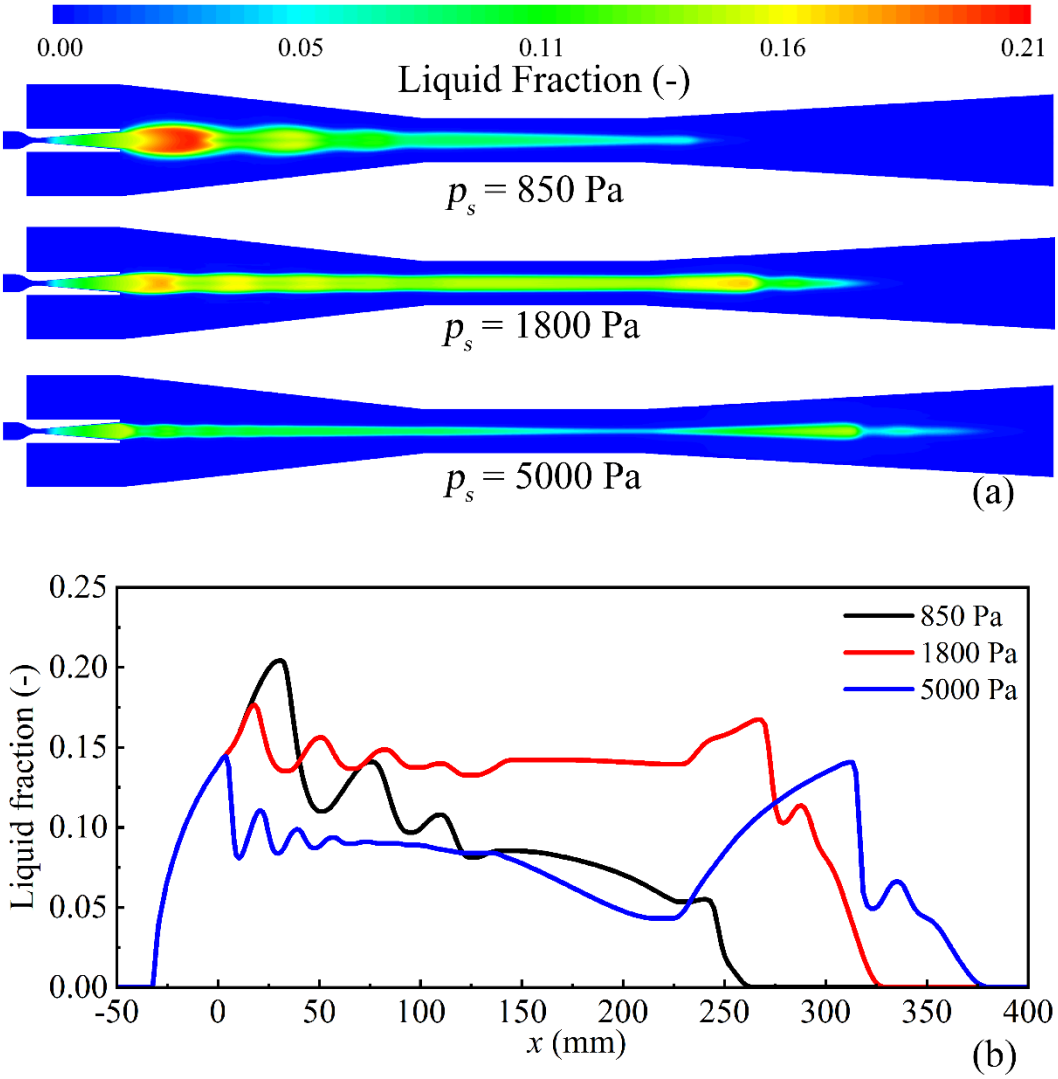

Fig. 10 Impacts of the suction chamber pressure on nonequilibrium condensations in under-expanded and over-expanded flows inside the steam ejector: (a) contours and (b) profiles of the liquid fraction

3.4. Performance evaluation of the steam ejector

The entrainment ratio, ξ, is one of the promising parameters to assess the steam ejector in MED-TVC desalination systems [47], which is defined as the ratio of the mass flow rate of the secondary flow, m_{sec}, to the primary flow, m_{pri}.

$$\xi = \frac{m_{suc}}{m_{pri}} \tag{8}$$

The entrainment ratios represent the capacity of an ejector to entrain the low-pressure steam from the last effect in MED-TVC units. The impacts of the suction chamber pressure on entrainment ratios are described in Fig. 11. We see that the increasing suction chamber pressure improves the entrainment ratio, which is approximately 0.25 when the suction chamber pressure is fixed at 850 Pa for an under-expanded flow. If the over-expanded flow is achieved by assigning the suction chamber pressure at 5000 Pa, the entrainment ratio will enormously increase to 1.69. This means that the transition of the flow structure from an under-expanded flow to an over-expanded flow can entrain more steam from the last effect of the MED-TVC desalination system.

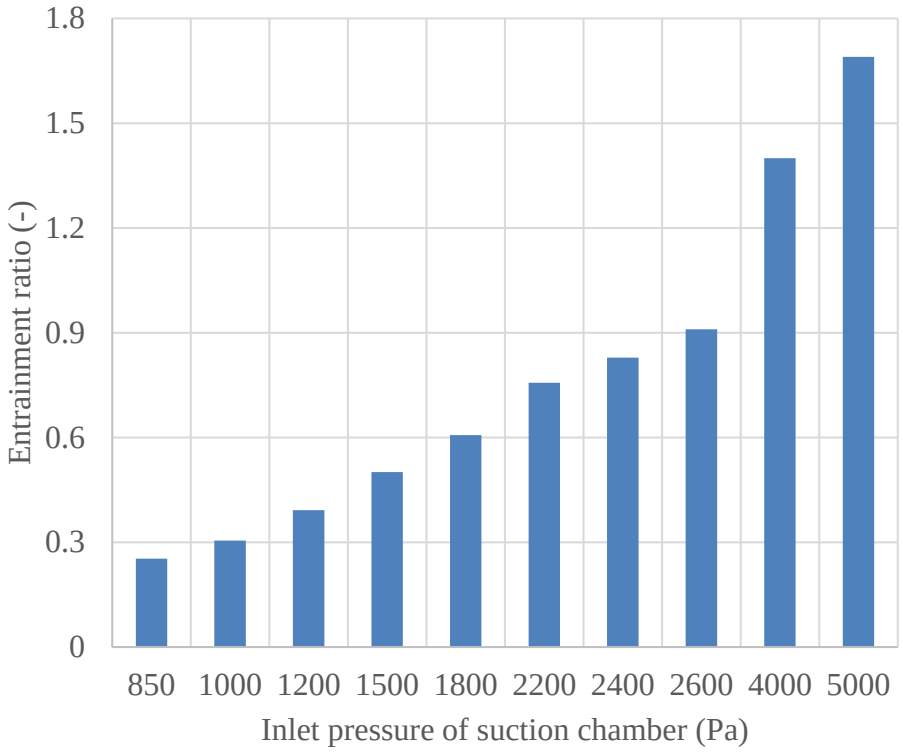

Fig. 11 Impact of the suction chamber pressure on the entrainment ratio of the steam ejector in the MED-TVC desalination system

The condensation-evaporation processes of the condensed droplets in the steam ejector are expected to affect the energy loss. The entropy loss coefficients [48], η, defined in Eq. (9) are utilised to assess the ejector energy loss in the MED-TVC desalination system. Figure 12 illustrates the entropy loss at various suction chamber pressures inside the steam ejector. We observe that the entropy loss coefficient increases with the rises of the suction chamber pressure. The entropy loss coefficient is approximately 0.081 when the pressure is fixed to 850 Pa at the suction chamber entrance. If the suction chamber pressure increases to 5000 Pa, the entropy loss coefficient will dramatically increase to 0.29. This indicates that the transition of the flow structures from an under-expanded flow to an over-expanded flow leads to a remarkable increase of the entropy loss in the steam ejector.

$$\eta = \frac{h_{in} - h_{out}}{h_{in} - h_{out} + T_{v,out}(s_{out} - s_{in})} \tag{9}$$

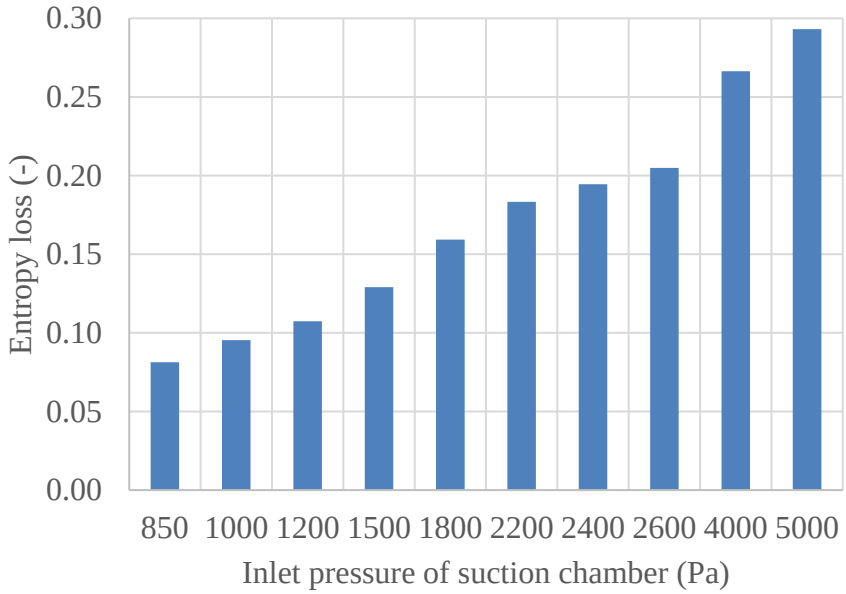

Fig. 12 Impact of the suction chamber pressure on the entropy loss in the steam ejector

4. Conclusions

The transition of the flow structure from an under-expanded flow to an over-expanded flow is investigated in a steam ejector for the multi-effect distillation with thermal vapour compression (MED-TVC) desalination system considering the condensation-evaporation processes of the massive droplets in supersonic flows. The maximum Mach number can reach 4.02 in an under-expanded flow and it is only approximately 2.88 in an over-expanded flow, which indicates that the expansion level of the steam is weakened by 28% in the steam ejector. The maximum liquid fraction decreases by 30% from 0.20 in the under-expanded flow to 0.14 in the over-expanded flow. The entrainment ratio and entropy loss coefficient both increase with the rises of the suction chamber pressure. This indicates that the transition of the flow structures from an under-expanded flow to an over-expanded flow can entrain more steam from the last effect while leads to a remarkable increase of the entropy loss in the steam ejector. This study reveals that the transition of the flow structure from the under-expanded flow to the over-expanded flow significantly affects the flow structure, condensation-evaporation of the massive droplets, entrainment ration and the entropy loss. It suggests that during the operation of the MED-TVC desalination system, the pressure of the last effect needs to be carefully controlled to achieve an under-expanded flow or an over-expanded flow in the steam ejector to improve the energy efficiency of the whole system.

Acknowledgements

This project has received funding from the European Union's Horizon 2020

research and innovation programme under the Marie Sklodowska-Curie grant agreement No 792876 and the National Natural Science Foundation of China under Grant 51876143.

References

[1] Andrés-Mañas J, Roca L, Ruiz-Aguirre A, Acién F, Gil JD, Zaragoza G. Application of solar energy to seawater desalination in a pilot system based on vacuum multi-effect membrane distillation. Applied Energy. 2020;258:114068.

[2] Colmenar-Santos A, Palomo-Torrejón E, Mur-Pérez F, Rosales-Asensio E. Thermal desalination potential with parabolic trough collectors and geothermal energy in the Spanish southeast. Applied Energy. 2020;262:114433.

[3] Tang Y, Liu Z, Shi C, Li Y. A novel steam ejector with pressure regulation to dredge the blocked entrained flow for performance improvement in MED-TVC desalination system. Energy Conversion and Management. 2018;172:237-47.

[4] Samaké O, Galanis N, Sorin M. Thermo-economic analysis of a multiple-effect desalination system with ejector vapour compression. Energy. 2018;144:1037-51.

[5] Catrini P, Cipollina A, Micale G, Piacentino A, Tamburini A. Exergy analysis and thermoeconomic cost accounting of a Combined Heat and Power steam cycle integrated with a Multi Effect Distillation-Thermal Vapour Compression desalination plant. Energy Conversion and Management. 2017;149:950-65.

[6] Elsayed ML, Mesalhy O, Mohammed RH, Chow LC. Exergy and thermo-economic analysis for MED-TVC desalination systems. Desalination. 2018;447:29-42.

[7] Askari IB, Ameri M. Techno economic feasibility analysis of Linear Fresnel solar

field as thermal source of the MED/TVC desalination system. Desalination. 2016;394:1-17.

[8] Khalid KA, Antar MA, Khalifa A, Hamed OA. Allocation of thermal vapor compressor in multi effect desalination systems with different feed configurations. Desalination. 2018;426:164-73.

[9] Tashtoush BM, Moh'd A A-N, Khasawneh MA. A comprehensive review of ejector design, performance, and applications. Applied Energy. 2019;240:138-72.

[10] Wen C, Rogie B, Kærn MR, Rothuizen E. A first study of the potential of integrating an ejector in hydrogen fuelling stations for fuelling high pressure hydrogen vehicles. Applied Energy. 2020;260:113958.

[11] Guimard L, Cipollina A, Ortega-Delgado B, Micale G, Couenne F, Bandelier P, et al. New considerations for modelling a MED-TVC plant under dynamic conditions. Desalination. 2019;452:94-113.

[12] Strušnik D, Marčič M, Golob M, Hribernik A, Živić M, Avsec J. Energy efficiency analysis of steam ejector and electric vacuum pump for a turbine condenser air extraction system based on supervised machine learning modelling. Applied Energy. 2016;173:386-405.

[13] Strušnik D, Golob M, Avsec J. Effect of non-condensable gas on heat transfer in steam turbine condenser and modelling of ejector pump system by controlling the gas extraction rate through extraction tubes. Energy Conversion and Management. 2016;126:228-46.

[14] Sharifi N, Boroomand M. An investigation of thermo-compressor design by

analysis and experiment: Part 1. Validation of the numerical method. Energy Conversion and Management. 2013;69:217-27.

[15] Sharifi N, Boroomand M. An investigation of thermo-compressor design by analysis and experiment: Part 2. Development of design method by using comprehensive characteristic curves. Energy Conversion and Management. 2013;69:228-37.

[16] Xue H, Wang L, Jia L, Xie C, Lv Q. Design and investigation of a two-stage vacuum ejector for MED-TVC system. Applied Thermal Engineering. 2020;167:114713.

[17] Han B, Liu Z, Wu H, Li Y. Experimental study on a new method for improving the performance of thermal vapor compressors for multi-effect distillation desalination systems. Desalination. 2014;344:391-5.

[18] Tang Y, Liu Z, Shi C, Li Y. A novel steam ejector with pressure regulation to optimize the entrained flow passage for performance improvement in MED-TVC desalination system. Energy. 2018;158:305-16.

[19] Tang Y, Liu Z, Li Y, Shi C, Lv C. A combined pressure regulation technology with multi-optimization of the entrainment passage for performance improvement of the steam ejector in MED-TVC desalination system. Energy. 2019;175:46-57.

[20] Wang C, Wang L, Wang X, Zhao H. Design and numerical investigation of an adaptive nozzle exit position ejector in multi-effect distillation desalination system. Energy. 2017;140:673-81.

[21] Park IS. Numerical investigation of entraining performance and operational

robustness of thermal vapor compressor having swirled motive steam inflow. Desalination. 2010;257:206-11.

[22] Gu W, Wang X, Wang L, Yin X, Liu H. Performance investigation of an auto-tuning area ratio ejector for MED-TVC desalination system. Applied Thermal Engineering. 2019;155:470-9.

[23] Liu J, Wang L, Jia L, Wang X. The influence of the area ratio on ejector efficiencies in the MED-TVC desalination system. Desalination. 2017;413:168-75.

[24] Wang K, Wang L, Jia L, Cai W, Gao R. Optimization design of steam ejector primary nozzle for MED-TVC desalination system. Desalination. 2019;471:114070.

[25] Sharifi N, Boroomand M, Sharifi M. Numerical assessment of steam nucleation on thermodynamic performance of steam ejectors. Applied Thermal Engineering. 2013;52:449-59.

[26] Mazzelli F, Giacomelli F, Milazzo A. CFD modeling of condensing steam ejectors: Comparison with an experimental test-case. International Journal of Thermal Sciences. 2018;127:7-18.

[27] Tang Y, Liu Z, Li Y, Wu H, Zhang X, Yang N. Visualization experimental study of the condensing flow regime in the transonic mixing process of desalination-oriented steam ejector. Energy Conversion and Management. 2019;197:111849.

[28] Wen C, Ding H, Yang Y. Performance of steam ejector with nonequilibrium condensation for multi-effect distillation with thermal vapour compression (MED-TVC) seawater desalination system. Desalination. 2020;489:114531.

[29] Sriveerakul T, Aphornratana S, Chunnanond K. Performance prediction of steam ejector using computational fluid dynamics: Part 1. Validation of the CFD results. International Journal of Thermal Sciences. 2007;46:812-22.

[30] Sriveerakul T, Aphornratana S, Chunnanond K. Performance prediction of steam ejector using computational fluid dynamics: Part 2. Flow structure of a steam ejector influenced by operating pressures and geometries. International Journal of Thermal Sciences. 2007;46:823-33.

[31] Yang Y, Walther JH, Yan Y, Wen C. CFD modeling of condensation process of water vapor in supersonic flows. Applied Thermal Engineering. 2017;115:1357-62.

[32] Bian J, Cao X, Yang W, Song X, Xiang C, Gao S. Condensation characteristics of natural gas in the supersonic liquefaction process. Energy. 2019;168:99-110.

[33] Bian J, Cao X, Yang W, Guo D, Xiang C. Prediction of supersonic condensation process of methane gas considering real gas effects. Applied Thermal Engineering. 2020;164:114508.

[34] Wen C, Ding H, Yang Y. Optimisation study of a supersonic separator considering nonequilibrium condensation behaviour. Energy Conversion and Management. 2020;222:113210.

[35] Han X, Zeng W, Han Z. Investigating the dehumidification characteristics of the low-pressure stage with blade surface heating. Applied Thermal Engineering. 2020;164:114538.

[36] Wen C, Karvounis N, Walther JH, Ding H, Yang Y. Non-equilibrium condensation of water vapour in supersonic flows with shock waves. International Journal of

Heat and Mass Transfer. 2020;149:119109.

[37] Wen C, Karvounis N, Walther JH, Yan Y, Feng Y, Yang Y. An efficient approach to separate CO_2 using supersonic flows for carbon capture and storage. Applied Energy. 2019;238:311-9.

[38] Kantrowitz A. Nucleation in very rapid vapor expansions. The Journal of chemical physics. 1951;19:1097-100.

[39] Young J. The spontaneous condensation of steam in supersonic nozzle. Physico Chemical Hydrodynamics. 1982;3:57-82.

[40] ANSYS Fluent Theory Guide. ANSYS Inc, USA. 2017.

[41] Yang Y, Zhu X, Yan Y, Ding H, Wen C. Performance of supersonic steam ejectors considering the nonequilibrium condensation phenomenon for efficient energy utilisation. Applied Energy. 2019;242:157-67.

[42] Moses CA, Stein GD. On the growth of steam droplets formed in a Laval nozzle using both static pressure and light scattering measurements. Journal of Fluids Engineering. 1978;100:311-22.

[43] Starzmann J, Hughes FR, Schuster S, White AJ, Halama J, Hric V, et al. Results of the International Wet Steam Modeling Project. Proceedings of the Institution of Mechanical Engineers, Part A: Journal of Power and Energy. 2018;232:550-70.

[44] Gürbüz H, Buran D. Experimental study on the effect of concentrated turbulence around the spark plug zone in a swirling flow on a hydrogen SI engine performance and combustion parameters. Journal of Energy Engineering. 2016;142:04015031.

[45] Gürbüz H. Experimental evaluation of combustion parameters with ion-current

sensor integrated to fast response thermocouple in SI engine. Journal of Energy Engineering. 2017;143:04016046.

[46] Solmaz Ö, Gürbüz H, Karacor M. Comparison of Artificial Neural Network and Fuzzy Logic Approaches for the Prediction of In-Cylinder Pressure in a Spark Ignition Engine. Journal of Dynamic Systems, Measurement, and Control. 2020;142:091005.

[47] Tang Y, Liu Z, Li Y, Yang N, Wan Y, Chua KJ. A double-choking theory as an explanation of the evolution laws of ejector performance with various operational and geometrical parameters. Energy Conversion and Management. 2020;206:112499.

[48] Dykas S, Majkut M, Smołka K, Strozik M. Study of the wet steam flow in the blade tip rotor linear blade cascade. International Journal of Heat and Mass Transfer. 2018;120:9-17.